*Journal of Enzyme Inhibition and Medicinal Chemistry*, February 2009; 24(1): 38–46



# His22 of TLXI plays a critical role in the inhibition of glycoside hydrolase family 11 xylanases

SIGRID ROMBOUTS[1], ELLEN FIERENS[2], ELIEN VANDERMARLIERE[3], ARNOUT VOET[4], KURT GEBRUERS[2], JOHNNY BEAUGRAND[2], CHRISTOPHE M. COURTIN[2], JAN A. DELCOUR[2], MARC DE MAEYER[4], ANJA RABIJNS[3], STEVEN VAN CAMPENHOUT[1], & GUIDO VOLCKAERT[1]

[1]*Laboratory of Gene Technology, Katholieke Universiteit Leuven, Kasteelpark Arenberg 21, B-3001 Leuven, Belgium,* [2]*Laboratory of Food Chemistry and Biochemistry, Katholieke Universiteit Leuven, Kasteelpark Arenberg 20, B-3001 Leuven, Belgium,* [3]*Laboratory for Biocrystallography, Katholieke Universiteit Leuven, Herestraat 49, B-3000 Leuven, Belgium, and* [4]*Laboratory of Biomolecular Modeling and BioMacS, Katholieke Universiteit Leuven, Celestijnenlaan 200G, B-3001 Leuven, Belgium*

(*Received 18 June 2007; accepted 10 November 2007*)



**Abstract**

Recently, a novel wheat thaumatin-like protein, TLXI, which inhibits microbial glycoside hydrolase family (GH) 11 xylanases has been identified. It is the first xylanase inhibitor that exerts its inhibition in a non-competitive way. In the present study we gained insight into the interaction between TLXI and xylanases via combined molecular modeling and mutagenic approaches. More specifically, site-specific mutation of His22, situated on a loop which distinguishes TLXI from other, non-inhibiting, thaumatin-like proteins, and subsequent expression of the mutant in *Pichia pastoris* resulted in a protein lacking inhibition capacity. The mutant protein was unable to form a complex with GH11 xylanases. Based on these findings, the interaction of TLXI with GH11 xylanases is discussed.

**Keywords:** *Thaumatin-like protein, xylanase inhibitor, protein–protein interaction, site-directed mutagenesis,* Pichia pastoris

## Introduction

Endoxylanases (EC 3.2.1.8) (further referred to as xylanases) are hydrolytic enzymes involved in the degradation of arabinoxylans. These cell wall polysaccharides mainly found in cereal grains, are quality determining factors in several cereal-based biotechnological processes such as the production of bread [1–2] and pasta [3]. Therefore xylanases are used as an additive in these different processes [4–5]. The majority of the xylanases belong either to glycoside hydrolase family 10 (GH10) or to the structurally unrelated glycoside hydrolase family 11 (GH11) ([6] http://afmb.cnrs-mrs.fr/CAZY/). In both families, a pair of glutamate residues catalyzes the cleavage of the glycosidic bond, one acting as a nucleophile and the other as the acid–base catalyst. Recently, a xylanase was shown to be indispensable in the infection of plants by the pathogen *Botrytis cinerea* [7]. Not only microorganisms, but also plants produce xylanases. The latter belong to GH10 and play important physiological roles in several tissues, such as contribution to seed germination and fruit ripening [8].

In the last decade, three structurally different types of proteinaceous inhibitors of these enzymes were discovered in wheat: TAXI- (*Triticum aestivum* xylanase inhibitor) [9,10], XIP- (xylanase inhibitor

Correspondence: G. Volckaert, Laboratory of Gene Technology, Katholieke Universiteit Leuven, Kasteelpark Arenberg 21, B-3001 Leuven, Belgium. Tel: 32 16 329667. Fax: 32 16 321965. E-mail: guido.volckaert@biw.keleuven.be

ISSN 1475-6366 print/ISSN 1475-6374 online © 2009 Informa UK Ltd.
DOI: 10.1080/14756360701841913

protein) [11] and TLXI- (thaumatin-like xylanase inhibitor) type inhibitors [12]. The practical significance of inhibition in several cereal-based processes has been reviewed [13].

TAXI-type inhibitors are active against microbial GH11 xylanases [14]. Recent crystallographic data of an *Aspergillus niger* xylanase-TAXI-I complex revealed both a direct interaction of the inhibitor with the active site region of the enzyme as well as substrate-mimicking contacts filling the whole substrate-docking region [15]. His374 turned out to be a key residue in xylanase inhibition and its role in enzyme–inhibitor interaction was confirmed by site-directed mutagenesis [16].

XIP-type inhibitors inhibit xylanases from microbial origin, irrespective of whether they belong to GH10 or GH11. The crystal structures of XIP-I in complex with GH10 *A. nidulans* xylanase and GH11 *P. funiculosum* xylanase have been solved [17]. From the results, it appeared that XIP-I contains two independent enzyme-binding sites, which allow substrate mimicry-based binding to GH10 and GH11 xylanases, respectively. The key elements in the inhibition are Lys234 and Arg149, respectively.

To date, nothing is known about the interaction mechanism between xylanases and the non-competitive xylanase inhibitor, TLXI [12] (Genbank no. *AJ786601*). Except for zeamatin, an α-amylase/trypsin inhibitor from maize (*Zea mays*) [18], no enzyme inhibitor is currently known among the thaumatin-like proteins (TLPs). Here, a 3D-model of TLXI was used as the basis for a mutagenic approach to elucidate the interaction mechanism with a GH11 xylanase. We focused on basic residues on the surface of TLXI because, for both TAXI-I and XIP, basic residues play a key role in the interaction with GH11 xylanases. Among these, two histidine residues (His10 and His22) were selected for mutagenesis based on a comparison with the TAXI-I sequence and with other TLPs, respectively. Only mutation of His22, located on a loop connecting two β-strands, which is more extensive and flexible as compared to other TLPs, abolished inhibition activity. The loss of inhibition capacity was shown to be caused by the inability of the mutant to form a complex with the tested xylanases.

## Materials and methods

### *Site-directed mutagenesis*

Mutations (H10A, H22A) were introduced via the "megaprimer" method [19] using H10Af (5′-AACCG-TTGCGCCTTCACGGTG-3′) and H22Af (5′-CTC-GTGCTCGCCC-AAGGGGGC-3′) as mutagenic primers (mutagenic bases are underlined). The 'megaprimer' was constructed with the mutagenic primer in combination with XImatr (5′-CAC**AGATCT**TCATG-GGCAGAAGACGATCTG-3′) (*Bgl*II restriction sites are shown in bold). This PCR reaction was performed with *Pfu* DNA polymerase (Fermentas, Burlington, Canada) (1.25 U) using a pCR®4-TOPO® (Invitrogen, Carlsbad, USA) construct containing the *tlxi* gene [12] as a template (1.5 ng), 200 μM of each dNTP, 3 μl commercially supplied (10 ×) buffer and 0.6 μM of each primer. PCR conditions were: 5 min at 95°C; 1 min at 95°C, 1 min 30 s at 58°C, 2 min at 72°C (35 cycles); and 15 min at 72°C. The PCR products were purified (Qiagen, Hilden, Germany) and used as a 'megaprimer" in a subsequent amplification reaction in combination with XImatf (5′-CACAGATCTGCACCGCTCACC-ATCACGAAC-3′) or M13r (5′-CAGGAAACAG-CTAT-GAC-3′) (in case of H10A), the latter annealing to the pCR®4-TOPO® vector template. The reaction mixtures containing 1.5 ng template, 200 μM of each dNTP, 3.0 μl of commercially supplied (10 ×) buffer, 1.25 U *Pfu* DNA polymerase and 300 ng megaprimer, were subjected to incubation at 95°C for 1 min and 72°C for 3 min (5 cycles). At this point the flanking primer (XImatf/M13r) was added and 25 cycles at 95°C for 1 min, 58°C for 1 min 30 s, 72°C for 1 min were followed by a final extension at 72°C for 15 min. For H10A, an annealing temperature of 60°C was used. Prior to cloning in a pCR®4-TOPO® vector, PCR products were gel extracted (QIAquick Gel Extraction Kit, Qiagen) and 3′deoxyadenylate-overhangs were added with *SuperTaq* polymerase (SphaeroQ, Leiden, The Netherlands) (2.5 U, 72°C, 10 min). After sequence verification, the *tlxi* gene containing the desired mutation was subcloned as a *Bgl*II fragment in the *Bsm*BI site of a pPICZαC expression vector (Invitrogen) as described in [12]. The ligation mixture was used to transform *Escherichia coli* TOP10 cells (Invitrogen).

### *Recombinant expression and purification*

Sequence-verified pPICZαC constructs were linearized with *Pme*I (New England Biolabs, Beverly, MA, USA) and subsequently used to transform *Pichia pastoris* strain X33 according to the EasyComp Transformation protocol (Invitrogen manual). For both mutants ($rTLXI_{[H10A]}$ and $rTLXI_{[H22A]}$) small scale expression (1.0 ml) was performed according to Shi and co-workers [20]. Large-scale expression and purification of recombinant TLXI (rTLXI) and $rTLXI_{[H22A]}$ were performed according to [12].

### *Protein content determination and circular dichroism*

Protein concentrations were determined spectrophotometrically at 280 nm using a specific absorbance value of 1.402 AU and 1.407 AU for 1 mg/ml rTLXI and $rTLXI_{[H22A]}$, respectively (1.000 cm UV-cell path length). Circular dichroism (CD) was performed as described in [16]. Pure protein samples were prepared in 25 mM sodium acetate buffer (pH 5.0) at concentratrions of 15.0 μM.

```
                CEEEEEECCCCCEEEEEECCCCEEEEEEEECCCCEEEEECCCCCCCEEE
Thaumatin       ATFEIVNRCSYTVWAAASKGDAALDAGGRQLNSGESWTINVEPGTNGGKI 50
                |   | |||  ||| |          ||  |  | ||           |
TLXI            APLTITNRCHFTVWPAVALVLH-QGGGGTELHPGASWSLDTPVI-GSQYI 48
                CCEEEEECCCCCEECEECCCCC-CCCCCCCCCCCCCEEEEECCCC-CEEEE

                EEEEEEEECCCCCEEEEECCCCC-CCCCCCCCCCCCCEEEEEEEECCEEE
Thaumatin       WARTDCYFDDSGSGICKTGDCGG-LLRCKRFGRPPTTLAEFSLNQYGKDY 99
                | || | ||  | | | ||||||    |      | | || |  |    |
TLXI            WGRTGCSFDRAGKGRCQTGDCGGSSLTCGGNPAVPVTMAEVSVLQGNYTY 98
                EECCCCCCCCCCCCCCCCCCCCCCEEECCCCCCCCCCCEEEEEECCCCCE

                EEEECCCCCCCCEEEEECCCCCCCEEECCCHHHHCCCCCCCCCCCCCCHH
Thaumatin       IDISNIKGFNVPMDFSPTTRGCRGVRCAADIVGQCPAKLKAPGGGCNDAC 149
                   |  |||| |||          | |
TLXI            GVTSTLKGFNLPMDLKCSSGDALPCRKA---------------------- 128
                EEEECCCCCCCEEEEEECCCCCCCCCCC----------------------

                HHHCCHHHHCCCCCCCCCHHHHHHHHHCCCEECCCCCCCCCEEEECCCCE
Thaumatin       TVFQTSEYCCTTGKCGPTEYSRFFKRLCPDAFSYVLDKPTTVTCPGSSNY 200
                                                  |            |
TLXI            -------------------------------GCDVVQPYAKSCSAAGSRL 145
                -------------------------------CCCCCCCCCCCCCCCCCCC

                EEEECCCC
Thaumatin       RVTFCPTA
                   |||
TLXI            QIVFCP--
                CEECCC—
```

Figure 1. Alignment of TLXI with thaumatin used to create the structure model of TLXI with the thaumatin structure as template. The sequence-alignment is provided by the genthreader threading algorithm [24]. C stands for coil, H for helix and E for extended sheet.



*Western blot*

Polyclonal antibodies raised against native TLXI, obtained from rabbit immunization and purified by affinity chromatography, were used for western blot analysis of native TLXI isolated from wheat (0.5 μg), rTLXI (0.56 μg) and $rTLXI_{[H22A]}$ (0.45 μg) according to Beaugrand et al. [21].

*Xylanase inhibition activity measurements*

Xylanase inhibition activities were determined with the colorimetric Xylazyme-AX method as previously described [22] using *A. niger* xylanase (ExlA, GenBank no. *CAA01470*) and *Trichoderma reesei* xylanase (XynI, GenBank no. *CAA49294*) from Megazyme (Bray, Ireland). One enzyme unit corresponds to the amount of enzyme leading to an increase in absorbance (590 nm) of one with the Xylazyme-AX method in the absence of inhibitor. Inhibition activity was expressed as percentage reduction of xylanase activity. All inhibition activity measurements were performed in triplicate at pH 5.0 (25.0 mM sodium acetate) and 40°C, the optimal conditions for inhibition activity, as previously determined [12].

*Gel permeation chromatography (GPC)*

To assess complex formation, GPC on a Bio-Silect SEC 125-5 column (300 × 7.8 mm) (Bio-Rad, Hercules, CA, USA) was performed, followed by SDS-PAGE analysis. Purified rTLXI and $rTLXI_{[H22A]}$ were freeze-dried and dissolved in 250 mM sodium acetate buffer (pH 5.0). ExlA and XynI were dialyzed overnight against the same buffer. Following samples, prepared in 150 μl of 250 mM sodium acetate buffer (pH 5.0), were loaded separately on the column: ExlA (80 μg), XynI (46.5 μg), rTLXI (20 μg) and $rTLXI_{[H22A]}$ (17.6 μg).

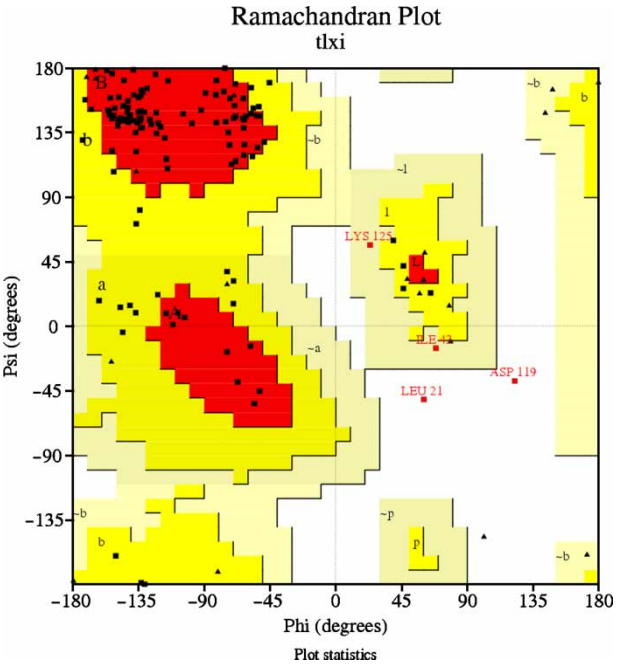


Figure 2. Ramachandran plot generated from the protein structure of TLXI, created with PROCHECK [25].

To investigate complex formation, the following samples were mixed and incubated for 30 min at room temperature followed by loading on the GPC column (molar ratios are indicated): ExlA and rTLXI (2.8:1), ExlA and rTLXI$_{[H22A]}$ (3.6:1), XynI and rTLXI (2.4:1), XynI and rTLXI$_{[H22A]}$ (2.2:1). GPC separation was performed at a flow rate of 1.0 ml/min and column calibration was done with the Gel Filtration LMW calibration kit (GE Healthcare, Uppsala, Sweden).

### *Modeling*

A molecular model of TLXI was generated with MOE (The Molecular Operating Environment) (Chemical Computing Group Inc., Montreal, Canada) using the structure of thaumatin (PDB code 1THV [23]) as template. The sequence-alignment provided by the genthreader threading algorithm [24] was adapted in order to obtain a better model. The model was visualized using Pymol (http://pymol.sourceforge.net/) and the stereochemical quality was verified with PROCHECK [25]. Two amino acids have unfavorable torsion angles (L21, D119); these amino acids are present in a fragment for which suitable alignment could be found. The exact alignment of the amino acid sequences of TLXI and thaumatin, including the structural features in which the amino acid are involved and the ramachandran plot of the model are shown in Figures 1 and 2, respectively.

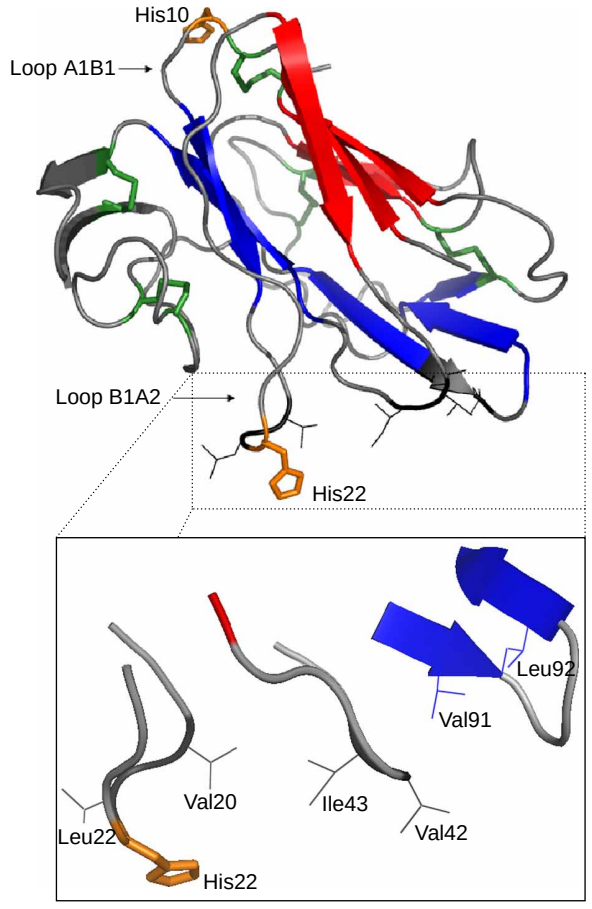


Figure 3. Ribbon diagram of the 3D-model of TLXI generated by MOE. The three β-sheets are in red, blue and grey. The five disulfide bridges are indicated in green. Amino acids histidine 10 and 22, are labeled. Loop names were assigned based on the topology diagram generated with TopDraw [26] and are as presented in Figure 1. The hydrophobic residues flanking His22 are indicated in stick format (black).

## Results and discussion

### *Identification of candidate key residues*

Based on the inhibition mechanism of TAXI and XIP, we speculated basic residues located at the surface to be prime candidates as key residues in the interaction of TLXI with xylanase enzymes. For this purpose, a 3D-model of TLXI was generated using MOE (see Figure 3), showing that the structure of TLXI consists of β-strands only (confirmed by CD analysis, cfr infra), organized in three β-sheets. Loop names were assigned based on the topology diagram generated with TopDraw [26] (see Figure 4). Eleven basic amino acid residues were revealed at the surface of the TLXI molecule. Among these, we focused on both His10 and His22.

Residue His10 residing on loop A1B1 was selected for mutagenesis because the triad His10-Phe11-Thr12 showed a remarkable identity with the key residue containing TAXI-I segment His374-Phe375-Thr376. Residue His22 was chosen because, according to the

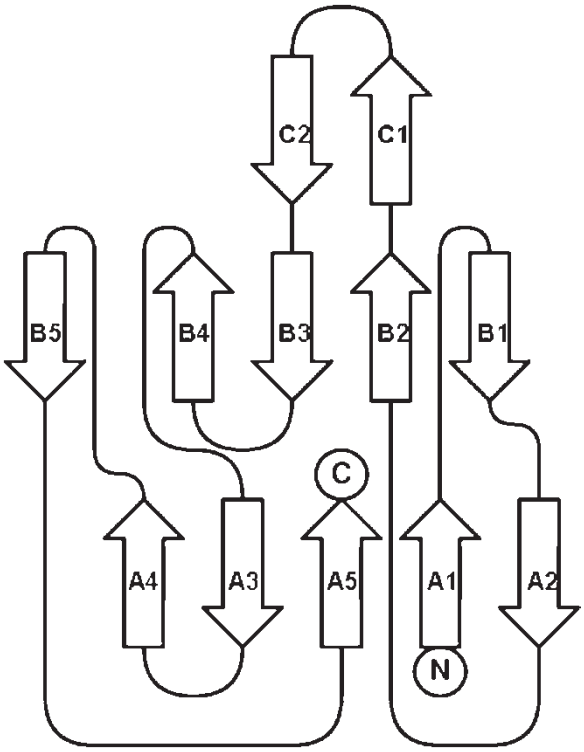


Figure 4. Topology diagram of the TLXI model made with TopDraw [26]. β-strands are presented as arrows. The thin lines correspond to loops. N-and C-terminal ends are indicated.

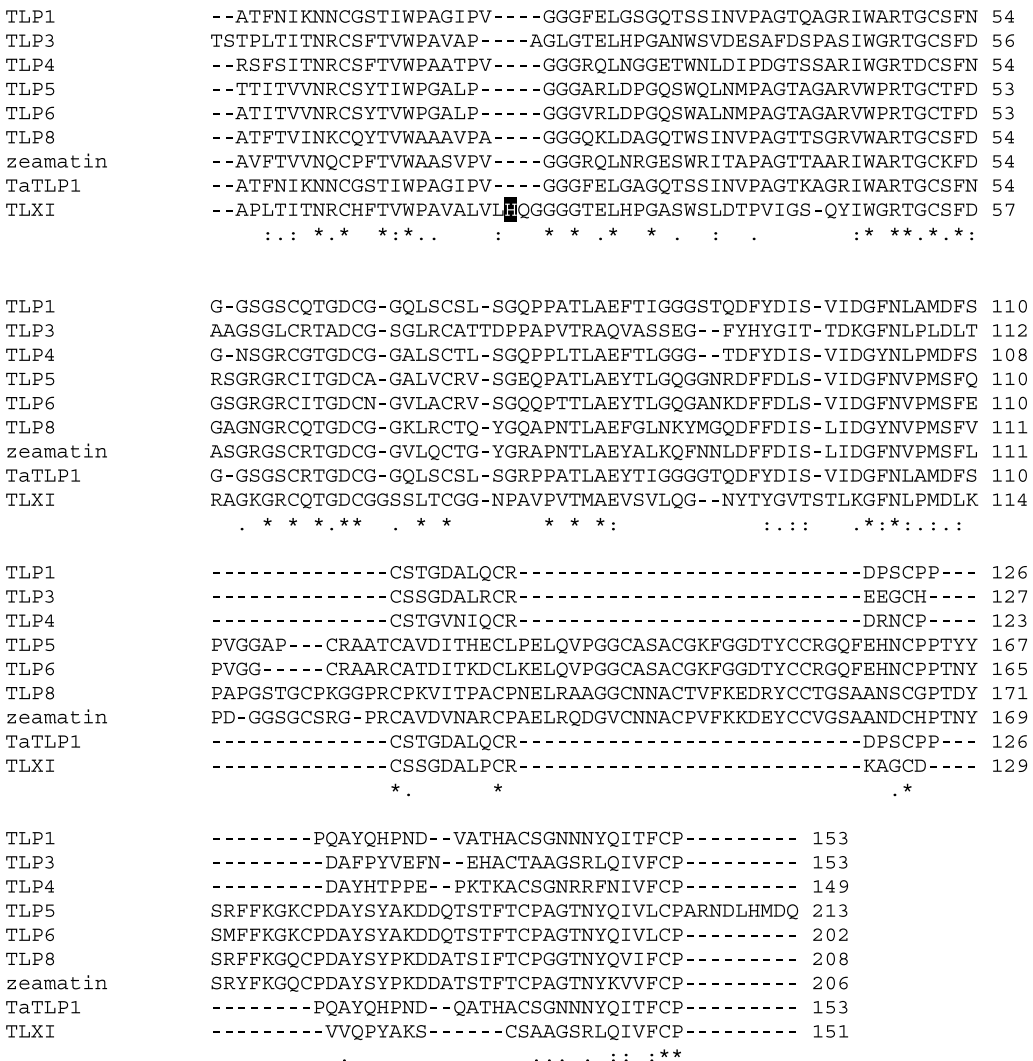


Figure 5. Alignment of TLXI with TLPs from cereal origin. His22 is shaded. TLP1, 3, 4, 5, 6 and 8 are from *Hordeum vulgare* (GenBank nos. *AY839292*, *AY839294*, *AF355455*, *AY838295*, *AF355456* and *AF355458*, respectively). Zeamatin and TaTLP1 are from *Zea Mays* and *T. aestivum*, respectively (GenBank nos. *U06831* and *AF384146*, respectively).

3D-model, it is located on a loop (B1A2) connecting two β-strands, which is longer than the loop of other TLPs from (cereal) origin (see Figures 3 and 5) and is more flexible due to the presence of several glycine residues. For thaumatin, possessing no basic residue containing flexible loop, no xylanase inhibition activity towards GH10 and GH11 xylanases was detected up to a molar excess of thaumatin over xylanase of 1000. No xylanase inhibition activity was also proven so far for other TLPs. This indicates that this loop might confer inhibition capacity to TLXI. Moreover, the presence of a patch of solvent exposed hydrophobic amino acids near His22 (Val20, Leu21, Val42, Ile43, Val91 and Leu92) (see Figures 3 and 5), suggests that this part of the protein could become buried upon complex formation.

Site-directed mutants, $rTLXI_{[H10A]}$ and $rTLXI_{[H22A]}$, were constructed, cloned in pPICZαC and expressed on a small scale in *P. pastoris* as in [20]. Inhibition activity was determined on the supernatant, showing that mutant $rTLXI_{[H10A]}$ clearly inhibited XynI and ExlA. In contrast, no inhibition activity could be measured for $rTLXI_{[H22A]}$.

### *The crucial role of His22 in inhibition*

To discover what caused the loss of inhibition activity of $rTLXI_{[H22A]}$, large scale expression [12] was performed for this mutant. This resulted in the efficient secretion of $rTLXI_{[H22A]}$ in the culture medium (ca. 4 mg/liter). The purified mutant did not show xylanase inhibition activity against either XynI or ExlA (see Figure 6). The fact that both proteins (rTLXI and $rTLXI_{[H22A]}$) had similar molecular masses (MM) on SDS-PAGE and, on Western blot, both interacted with polyclonal antibodies raised against native TLXI (results not shown),

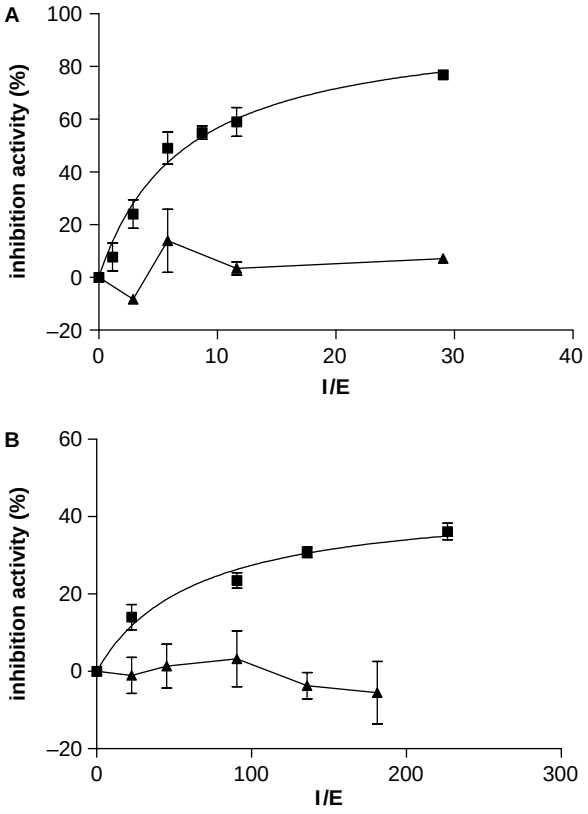


Figure 6. Inhibition activity measurements of rTLXI (■) and $rTLXI_{[H22A]}$ (▲) towards XynI (A) and ExlA (B) as a function of molar ratio (I/E). 1.0 unit of XynI or ExlA, respectively, was added to different amounts of rTLXI/ $rTLXI_{[H22A]}$ at pH 5.0 and the corresponding inhibition activity was determined using Xylazyme AX tablets as substrate.

showed that the purified proteins are indeed TLXI-type proteins. In addition, the similarity between the CD spectra of rTLXI and $rTLXI_{[H22A]}$ ruled out that the loss of inhibition activity was due to a change in secondary structure of the protein (see Figure 7).

To determine whether the H22A mutation abolished the capacity to form a complex with both GH11 xylanases, GPC was performed at pH 5.0. When the ExlA/rTLXI mixture was evaluated by GPC, a peak with a shoulder was eluted (see Figure 8A), the shoulder corresponding to the complex between rTLXI and ExlA (fraction 1 on SDS-PAGE). When rTLXI and ExlA were loaded separately on GPC, they eluted at a higher elution volume (see fraction 2 on SDS-PAGE, Figure 8A). Hence, the shift towards a lower elution volume, and thus a higher MM, is caused by complex formation of the two proteins. When the ExlA/ $rTLXI_{[H22A]}$ mixture was evaluated (see Figure 8B), only one peak was observed, which contained both free $rTLXI_{[H22A]}$ and free ExlA, because they have the same apparent MM on GPC. In this case, there was no shift towards a higher MM (fraction 1 on SDS-PAGE) and, hence, it can be concluded that no detectable amount of complex was formed. This conclusion was further supported by an analogous experiment with XynI

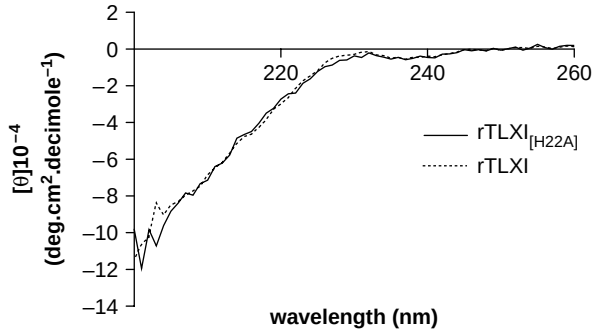


Figure 7. Circular dichroism spectra of rTLXI (dotted line) and $rTLXI_{[H22A]}$ (solid line). The spectra were normalized to the protein concentration and expressed as mean residue ellipticity [θ].

xylanase, the results paralleling those obtained with ExlA (see Figure 9).

### *Possible mechanism of inhibition*

Although XIP and TAXI were demonstrated to be competitive inhibitors [11,27] and TLXI was shown to be a non-competitive inhibitor [12], they seem to have in common that the key residue for inhibition is a surface exposed basic residue. Whereas crystallographic data are available for XIP and TAXI in complex with a xylanase [15,17], confirming the interaction in the active site, today, no such data are available for TLXI in complex with a xylanase. Hence, the present study provides a first insight in the inhibition determinants of TLXI. Since the TLXI protein inhibits xylanases in a non-competitive manner, it can be suggested that the interaction of TLXI with the xylanase occurs outside the active site. The precise interaction mechanism is, however, difficult to predict due to the uncertainty in both partners. Moreover, up to now few crystallographic data have been published about complex structures of enzymes with proteinaceous as well as chemical non-competitive inhibitors [28,29]. The general concept of a non-competitive inhibitor is that it induces a conformational change in the enzyme via binding to an allosteric site. The substrate would still be able to bind, but binding of the inhibitor hampers catalysis ($V_{max}$ decreases) through unfavourable repositioning of the catalytic residues. Work by Love and coworkers [29] suggested that a non-competitive inhibitor can also exert its activity by perturbing dynamic properties of a domain or interdomain contacts that are necessary for normal enzymatic function. They also postulated that such inhibitors can interfere with important protein—substrate interactions.

In order to formulate a hypothesis about the xylanase amino acid residues involved in the interaction with TLXI a close look was taken at the surface charges of two inhibited (XynI and ExlA) and two uninhibited (*T. longibrachiatum* XynII and *B. subtilis*

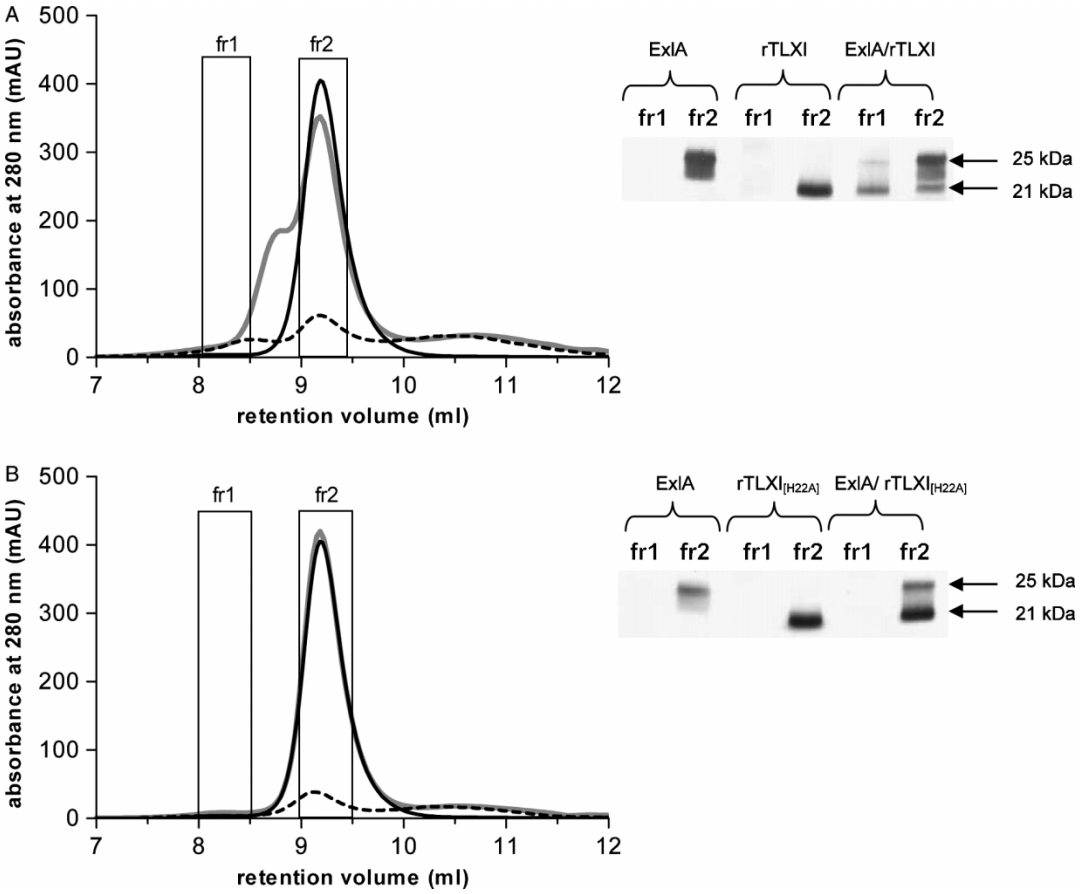


Figure 8. A) GPC of ExlA (solid black line), rTLXI (dashed black line) and ExlA/rTLXI (grey line) (incubated during 30 min at room temperature). The UV absorbance at 280 nm (mAU) is given as a function of the retention volume (ml). Fractions 1 and 2 are boxed. The major peak in the grey curve corresponds to the excess ExlA that was added. The corresponding SDS-PAGE is shown on the right and loaded fractions are indicated on top. The upper band (25 kDa) corresponds to ExlA, the lower band (21 kDa) corresponds to rTLXI. (B) GPC of ExlA (solid black line), $rTLXI_{[H22A]}$ (dashed black line) and $ExlA/rTLXI_{[H22A]}$ (grey line) (incubated during 30 min at room temperature) illustrated as above. The upper band corresponds to ExlA, the lower band corresponds to $rTLXI_{[H22A]}$.

XynA) xylanases (see Figure 7). The fact that inhibition activity is pH dependent [12] strongly indicates the involvement of electrostatic charges in the interaction. This is in line with the fact that His22, essential for inhibition and complex formation, carries a positive charge. We hence focused our efforts on negatively charged amino acids at the surface of ExlA and XynI, which are located outside the active site and are neutral or positively charged in the uninhibited xylanases. Two such residues were found: $Glu118_{ExlA}$ ($Glu112_{XynI}$) and $Asp85_{ExlA}$ ($Asp81_{XynI}$) (see Figure 10) which correspond to Ala and Ser in XynA and Gln and Asn in XynII, respectively. $Glu118_{ExlA}$ is located at the thumb of the xylanase. During the catalytic cycle, the thumb moves significantly and the active site is partly closed upon substrate binding. When the reaction proceeds, the thumb opens again and allows the reaction product to diffuse away [30]. Binding of TLXI to the thumb might hence perturb its dynamic properties thereby influencing the catalytic mechanism. Alternatively, interaction with the thumb region may sterically block

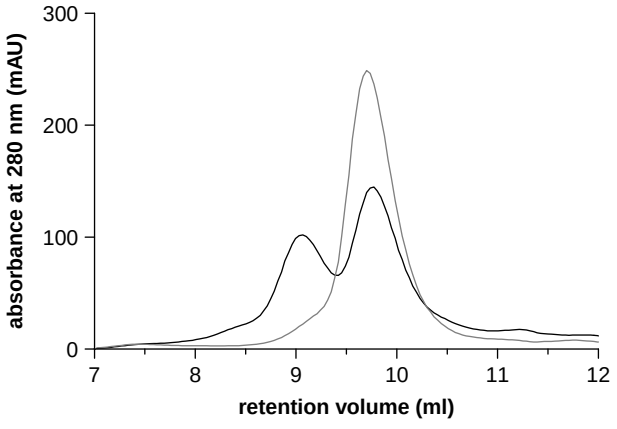


Figure 9. Comparison of GPC results of $XynI/rTLXI_{[H22A]}$ (grey) and XynI/rTLXI (black). The UV absorbance at 280 nm (mAU) is given as a function of the retention volume (ml). For XynI/rTLXI, the first peak corresponds to the complex, whereas the second peak represents the excess of XynI. For $XynI/rTLXI_{[H22A]}$ only one peak was observed corresponding to free XynI and $rTLXI_{[H22A]}$, having the same apparent MM on GPC.

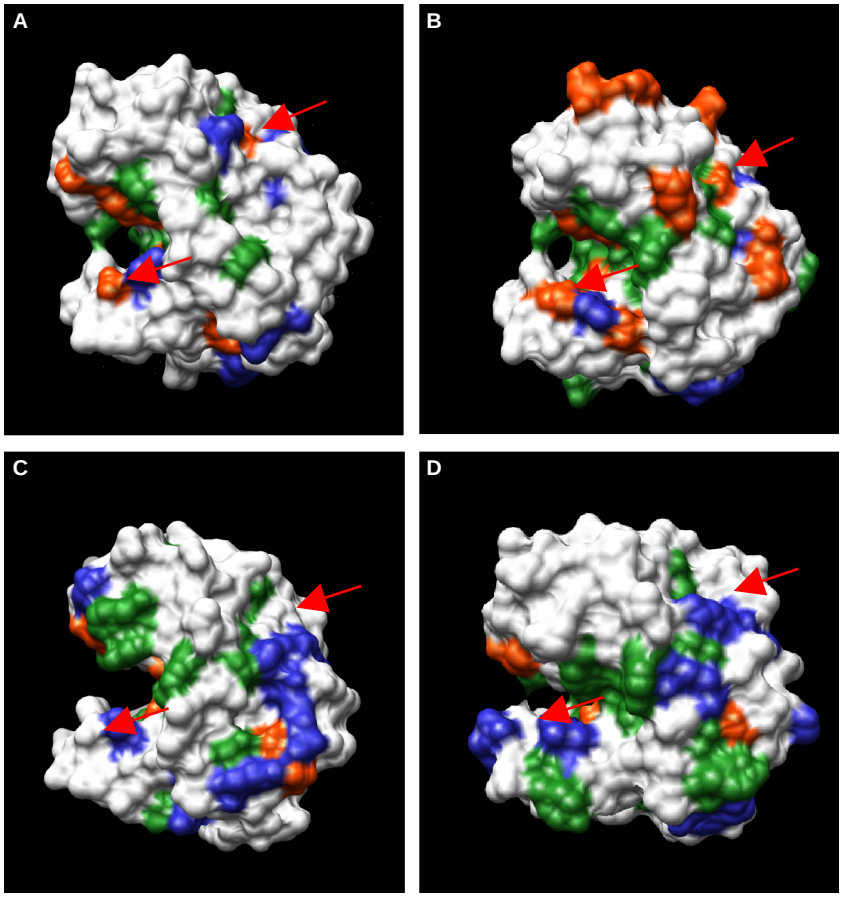


Figure 10. Solvent accessible surfaces of four GH11 xylanases. XynI (A) and ExlA (B) are inhibited by (r)TLXI. XynII (C) and XynA (D) (GenBank nos. *CAA49293* and *AAA22897*, respectively) are uninhibited by (r)TLXI. Negatively and positively charged residues and aromatic residues are indicated in red, blue and green, respectively. The upper arrow on each structure indicates the residues corresponding to $Glu118_{ExlA}$ whereas the lower arrow indicates the residues corresponding to $Asp85_{ExlA}$. Pictures were made with Chimera [32].

the entrance of substrate without directly interfering with the substrate binding sites. Increasing the substrate concentration in this case wouldn't decrease inhibition since substrate and inhibitor don't compete for the same binding sites, resulting in a non-competitive inhibition profile. In contrast, $Asp85_{ExlA}$ is located on the finger of the xylanase in the proximity of the hinge region between palm and fingers [30]. Interaction of TLXI with this region might perturb flexibility of the fingers influencing catalytic activity. However, the movement of the fingers during the catalytic cycle is not as pronounced as the movement of the thumb [31]. Evidently, it can not be excluded that TLXI, by interacting with one of these residues, causes a conformational change in the xylanase, resulting in a decreased catalytic activity.

## Acknowledgements

The authors gratefully acknowledge financial support from the "Fonds voor Wetenschappelijk Onderzoek-Vlaanderen" (F.W.O.-Vlaanderen, Belgium) (post-doctoral fellowship K. Gebruers, A. Rabijns and S. Van Campenhout), the "Instituut voor de aanmoediging van Innovatie door Wetenschap en Technologie in Vlaanderen" (I.W.T., Brussels, Belgium) (Scholarship to S. Rombouts, E. Fierens and A. Voet, Xylafun GBOU project funding) and the Research Fund K.U. Leuven (post-doctoral fellowship to J. Beaugrand and S. Van Campenhout). We thank E. Lorent for the helping hand with CD.

## References

[1] Courtin CM, Delcour JA. Physicochemical and bread-making properties of low molecular weight wheat derived arabinoxylans. J Agric Food Chem 1998;46:4066–4073.
[2] Courtin CM, Delcour JA. Arabinoxylans and endoxylanases in wheat flour bread-making. J Cereal Sci 2002;35:225–243.
[3] Ingelbrecht JA, Moers K, Abécassis J, Rouau X, Delcour JA. Influence of arabinoxylans and endoxylanases on pasta processing and quality. Production of high-quality pasta with increased levels of soluble fiber. Cereal Chem 2002;78:721–729.
[4] Romanowska I, Polak J, Janowska K, Bielecki S. The application of fungal endoxylanase in bread-making. Commun Agric Appl Biol Sci 2003;68:317–320.
[5] Polizeli ML, Rizzatti AC, Monti R, Terenzi HF, Jorge JA, Amorim DS. Xylanases from fungi: Properties and industrial applications. Appl Microbiol Biotechnol 2005;67:577–591.
[6] Henrissat B. A classification of glycosyl hydrolases based on amino acid sequence similarities. Biochem J 1991;280:309–316.

[7] Brito N, Espino JJ, Gonzalez C. The endo-beta-1,4-xylanase Xyn11A is required for virulence in *Botrytis cinerea*. Mol Plant Microbe Interact 2006;19:25–32.
[8] Simpson DJ, Fincher GB, Huang AHC, Cameron-Mills V. Structure and function of cereal and related higher plant (1 → 4)-β-xylan endohydrolases. J Cereal Sci 2002;37:111–127.
[9] Debyser W, Derdelinckx G, Delcour JA. Arabinoxylan solubilisation and inhibition of the barley malt xylanolytic system by wheat during brewing with wheat wholemeal adjunct: Evidence for a new class of enzyme inhibitors. J Am Soc Brew Chem 1997;55:153–156.
[10] Debyser W, Delcour JA. Inhibitors and xylanolytic and β-glucanolytic enzymes, Eur Pat Filed April 1997, further matter added April 1998, published as WO 98/49278.
[11] McLauchlan WR, Garcia-Conesa MT, Williamson G, Roza M, Ravestein P, Maat J. A novel class of protein from wheat which inhibits xylanases. Biochem J 1999;338:441–446.
[12] Fierens E, Rombouts S, Gebruers K, Courtin CM, Goesaert H, Brijs K, Beaugrand J, Volckaert G, Van Campenhout S, Proost P, Delcour JA. TLXI, a novel type of xylanase inhibitor from wheat (*Triticum aestivum*) belonging to the thaumatin family. Biochem J 2007;403:583–591.
[13] Sørensen JF, Kragh KM, Sibbesen O, Delcour J, Goesaert H, Svensson B, Tahir TA, Brufau J, Perez-Vendrell AM, Bellincampi D, D'Ovidio R, Camardella L, Giovane A, Bonnin E, Juge N. Potential role of glycosidase inhibitors in industrial biotechnological applications. Biochim Biophys Acta 2004;1696:275–287.
[14] Henrissat B. A classification of glycosyl hydrolases based on amino acid sequence similarities. Biochem J 1991;280:309–316.
[15] Sansen S, De Ranter CJ, Gebruers K, Brijs K, Courtin CM, Delcour JA, Rabijns A. Structural basis for inhibition of *Aspergillus niger* xylanase by *Triticum aestivum* xylanase inhibitor-I. J Biol Chem 2004;279:36022–36028.
[16] Fierens K, Gils A, Sansen S, Brijs K, Courtin CM, Declerck PJ, De Ranter CJ, Gebruers K, Rabijns A, Robben J, Campenhout S, Volckaert G, Delcour JA. His374 of wheat endoxylanase inhibitor TAXI-I stabilizes complex formation with glycoside hydrolase family 11 endoxylanases. FEBS J 2005;272:5872–5882.
[17] Payan F, Leone P, Porciero S, Furniss C, Tahir T, Williamson G, Durand A, Manzanares P, Gilbert HJ, Juge N, Roussel A. The dual nature of the wheat xylanase protein inhibitor XIP-I: Structural basis for the inhibition of family 10 and family 11 xylanases. J Biol Chem 2004;279:36029–36037.
[18] Schimoler-O'Rourke R, Richardson M, Selitrennikoff CP. Zeamatin inhibits trypsin and α-amylase activities. Appl Environ Microbiol 2001;67:2365–2366.
[19] Smith AM, Klugman KP. "Megaprimer" method of PCR-based mutagenesis: The concentration of megaprimer is a critical factor. Biotechniques 1997;22:438–442.
[20] Shi X, Karkut T, Chamankhah M, Alting-Mees M, Hemmingsen SM, Hegedus D. Optimal conditions for the expression of a single-chain antibody (scFv) gene in *Pichia pastoris*. Protein Expr Purif 2003;28:321–330.
[21] Beaugrand J, Gebruers K, Ververken C, Fierens E, Croes E, Goddeeris B, Courtin CM, Delcour JA. Antibodies against wheat xylanase inhibitors as tools for the selective identification of their homologues in other cereals. J Cereal Sci 2006;44:59–67.
[22] Fierens K, Geudens N, Brijs K, Courtin CM, Gebruers K, Robben J, Van Campenhout S, Volckaert G, Delcour JA. High-level expression, purification and characterization of recombinant wheat xylanase inhibitor TAXI-I secreted by the yeast *Pichia pastoris*. Protein Expr Purif 2004;37:39–46.
[23] Ko TP, Day J, Greenwood A, Mcpherson A. Structures of three crystal forms of the sweet protein thaumatin. Acta Crystallog D 1994;50:813–825.
[24] McGuffin LJ, Jones DT. Improvement of the GenTHREADER method for genomic fold recognition. Bioinformatics 2003;19:874–881.
[25] Laskowski RA, McArthur MW, Moss DS, Thornton JM. PROCHECK: A program to check the stereochemical quality of protein structures. J Appl Cryst 1993;26:283–291.
[26] Bond CS. TopDraw: A sketchpad for protein structure topology cartoons. Bioinformatics 2003;19:311–312.
[27] Gebruers K. Endoxylanase inhibitors in wheat (*Triticum aestivum* L.): Isolation, characterisation and use for endoxylanase purification [dissertation]. Leuven: Katholieke Universiteit Leuven; 2002. p 178.
[28] Pallarès I, Bonet R, Garcia-Castellanos R, Ventura S, Avilés FX, Vendrell J, Gomis-Rüth FX. Structure of human carboxypeptidase A4 with its endogenous protein inhibitor, latexin. Proc Natl Acad Sci USA 2005;102:3978–3983.
[29] Love RA, Parge HE, Yu X, Hickey MJ, Diehl W, Gao J, Wriggers H, Ekker A, Wang L, Thomson JA, Dragovich PS, Fuhrman SA. Crystallographic identification of a noncompetitive inhibitor binding site on the hepatitis C virus NS5B RNA polymerase enzyme. J Virol 2003;77:7575–7581.
[30] Muilu J, Törrönen A, Perakyla M, Rouvinen J. Functional conformational changes of endo-1,4-xylanase II from *Trichoderma reesei*: A molecular dynamics study. Proteins 1998;31:434–444.
[31] Havukainen R, Törrönen A, Laitinen T, Rouvinen J. Covalent binding of three epoxyalkyl xylosides to the active site of endo-1,4-xylanase II from *Trichoderma reesei*. Biochemistry 1996;35:9617–9624.
[32] Pettersen EF, Goddard TD, Huang CC, Couch GS, Greenblatt DM, Meng EC, Ferrin TE. UCSF Chimera—a visualization system for exploratory research and analysis. J Comput Chem 2004;25:1605–1612.